Journal of Organometallic Chemistry 1022 (2024) 123399

Contents lists available at ScienceDirect

Journal of Organometallic Chemistry

journal homepage: www.elsevier.com/locate/jorganchem

Effect of backbone linker (O vs NH) on the ability of pincer-supported nickel hydrides to reduce CO_2

Mahmood Ahmadianpoor, Patrick D. Pridemore, Jeanette A. Krause, Hairong Guan *

Department of Chemistry, University of Cincinnati, P.O. Box 210172, Cincinnati, OH 45221-0172, USA

ARTICLE INFO

Keywords:
Pincer ligand
Nickel hydride
CO_2 capture
Insertion reaction
Formate complex
Ligand effect

ABSTRACT

The reactivity of nickel hydrides supported by a pincer ligand often can be tuned by modifying the ligand at the three donor sites. In this study, ligand modification is made at the backbone, more specifically the linkers X and Y in {2,6-C_6H_3(XP^tBu_2)(YP^tBu_2)}NiH. Of the three nickel hydrides investigated herein, the PNCNP-pincer complex (X = Y = NH) is the most reactive one towards CO_2, whether it is for the rate of CO_2 capture from air or for the thermodynamic favorability of CO_2 insertion into the Ni–H bond. The POCOP-pincer complex (X = Y = O) is the least reactive hydride whereas the POCNP-pincer complex (X = O, Y = NH) is ranked in the middle. To have access to the hybrid pincer complex, an improved synthetic method for the proligand, *m*-C_6H_4(OP^tBu_2)(NHP^tBu_2), is also developed.

1. Introduction

Transition metal hydrides are often implicated in catalytic processes that convert CO_2 to formic acid, formate derivatives, or further reduced molecules such as acetals, methanol, and methane [1–3]. The mechanistic relevance has motivated many researchers to study the CO_2 chemistry of well-defined metal hydride complexes, which can provide useful guidelines for designing more efficient catalysts. One class of metal hydrides that have emerged as popular subjects for the reactivity studies are nickel hydrides [4,5]. The growing interests in these specific hydrides are primarily driven by the fact that nickel is an earth-abundant metal and the reality that a wide variety of nickel hydride complexes are synthetically accessible (Fig. 1).

It is important to point out that not all nickel hydride complexes are reactive to CO_2. Early studies focusing on trans-(Cy_3P)$_2$NiH(X) showed that **1**–**7** failed to react with CO_2 (1 atm) [6]. However, replacing the X-type ligand with the more σ-donating methyl or phenyl group resulted in rapid CO_2 insertion to yield a nickel formate complex, although the reaction of **8** was complicated by the formation of methane and ethane [7]. Cationic nickel hydrides typically display low or no reactivity towards CO_2, as demonstrated by the imine-ligated complex (**10**) [8] and the diphosphine-supported nickel hydrides (**11** and **12**) [9,10]. In 2010, we reported a nickel hydride stabilized by a phosphinite-based (or POCOP-type) pincer ligand (**13**) as an efficient catalyst for the reduction of CO_2 (1 atm) with boranes [11]. The key step, namely CO_2 insertion into the Ni–H bond, is fast and quantitative at room temperature. Subsequent reports by us and others suggest that the pincer scaffold can be altered in many ways (**13** → **14**–**23**) without drastically changing the activity of the NiH moiety. Proven structural modifications include the introduction of less bulky P-substituents [12], saturation of the central phenyl ring [13], replacement of the backbone linker (i.e., O) with CH_2 [14–16], NMe [17], or NH [18], and construction of a completely new pincer architecture based on the donor set (P,Si,P) [15] or (P,B,P) [19]. The computational work by Hazari and Kemp concluded that having a strong σ-donor trans to the hydride would render CO_2 insertion favorable, both kinetically and thermodynamically [15]. Consistent with this analysis, nickel hydrides supported by a PNP-type pincer ligand (**24**–**28**) [20–23] react very slowly with CO_2, requiring hours/days, heating, and/or a high CO_2 pressure to complete the insertion process. The cationic nickel hydrides **29** and **30** are inert to CO_2 [24], and so is the PN^3P*-pincer complex **31** [25,26]. Of particular note is that, under photochemical conditions, **28** undergoes abnormal CO_2 insertion to afford a NiC(O)OH complex [23]. The PSiNSiP-pincer supported nickel hydride (**32**) also shows a unique reaction pattern with CO_2, giving an N/O transposition product {κ^P,κ^P-O($SiMe_2CH_2P^tBu_2$)$_2$}NiH(NCO) [27]. To probe metal-metal cooperativity, the Janus POCOP-pincer complex **33** [28] and the Ni-Ga heterobimetallic complex **34** [29] have been developed; both react with CO_2 rapidly to give the corresponding nickel formate complexes.

* Corresponding author.
E-mail address: hairong.guan@uc.edu (H. Guan).

https://doi.org/10.1016/j.jorganchem.2024.123399
Received 12 August 2024; Received in revised form 16 September 2024; Accepted 18 September 2024
Available online 19 September 2024

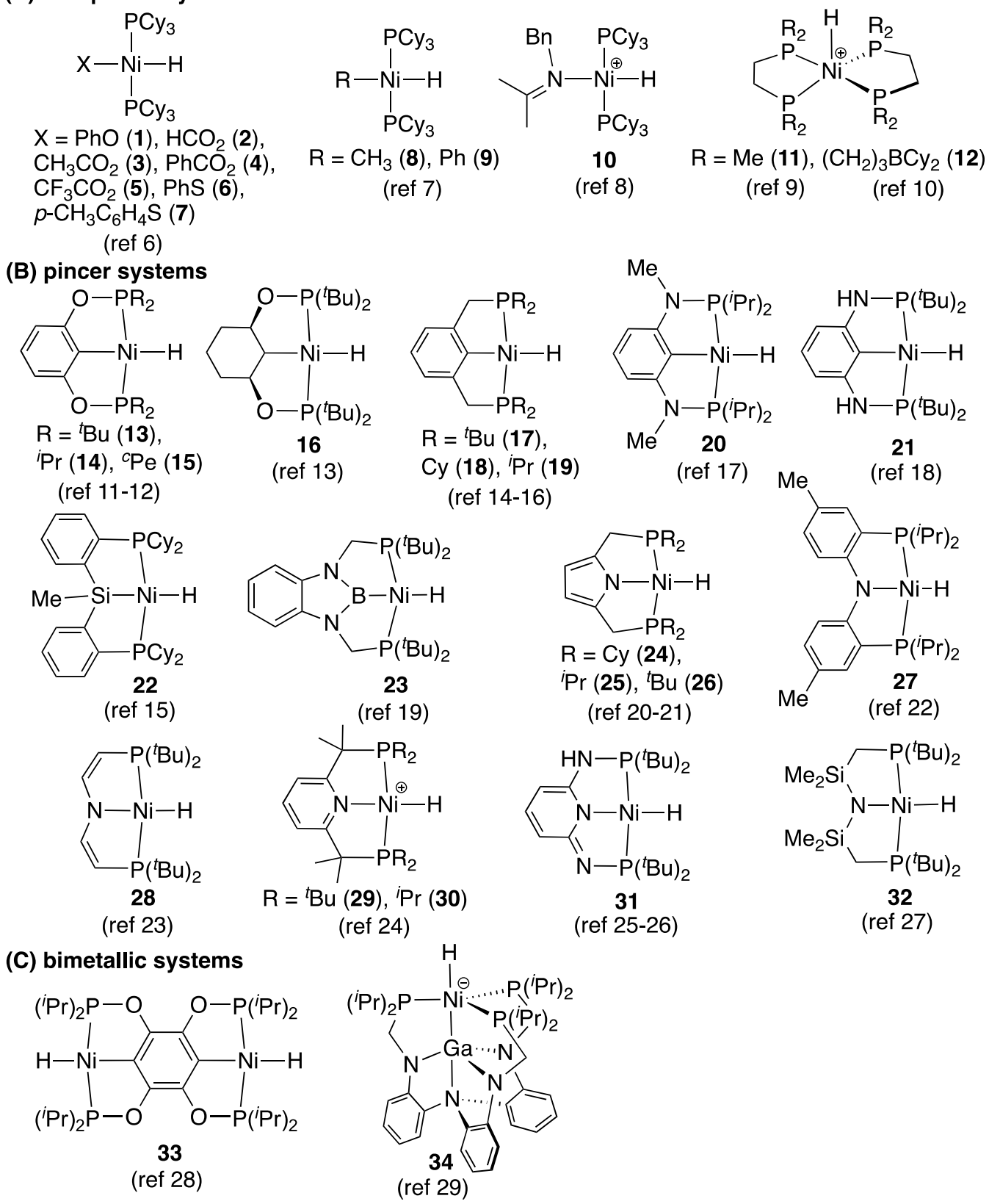

Fig. 1. Well-defined nickel hydride complexes studied for CO_2 reduction.

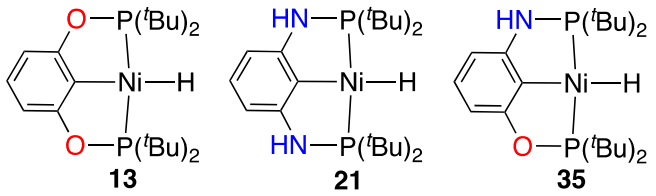

Fig. 2. Three pincer-supported nickel hydrides that differ by the backbone linker.

While informative, the results described above have invited more questions than answers pertaining to the structure-reactivity relationship. For example, how and to what extent would the P-substituents, backbone linker, and hybridization of the central carbon impact the reactivity of the nickel hydride? Some of these questions have already been addressed. Kinetics studies of CO_2 insertion with **17**–**19** revealed that the reaction was faster when the P-substituents became less sterically bulky [16]. Thermodynamically, the insertion reaction with **13**–**15** also appeared to be favored by smaller P-substituents [30]. In this work, we focus on the comparison of the POCOP-pincer complex **13** and the PNCNP-pincer complex **21** with the objective to understand how the ligand backbone linker (O vs NH) influences the ability of the nickel hydride to reduce CO_2. Considering that hybrid pincer complexes sometimes can be more effective catalysts [31,32], we have also included the POCNP-pincer complex **35** in this study (Fig. 2).

2. Results and discussion

2.1. Synthesis of POCNP-pincer complexes

The two nickel hydrides bearing a symmetric pincer ligand (i.e., **13** and **21**) were readily obtained using the synthetic procedures described in the literature [18,33]. The hybrid compound **35**, however, was challenging to make. The needed proligand, *m*-$C_6H_4(OP^tBu_2)(NHP^tBu_2)$, was previously prepared by the Liu group in two steps starting from *m*-aminophenol: (1) deprotonation of the OH and NH groups with *n*-BuLi (2 equiv) and (2) O–P and N–P bond formation with $^tBu_2PCl$ (2 equiv) in refluxing THF [34]. This method afforded the proligand with relatively low purity (~50%), which nevertheless still led to a successful synthesis of {2,6-$C_6H_3(OP^tBu_2)(NHP^tBu_2)$}Ir(H)Cl through cyclometalation with $[Ir(COE)_2Cl]_2$ (COE = cyclooctene). In contrast, attempts to use the impure proligand to perform cyclometalation with $NiCl_2$ failed to produce {2,6-$C_6H_3(OP^tBu_2)(NHP^tBu_2)$}NiCl (**35-Cl**, the precursor to **35**), suggesting that the unknown impurities interfered with the process of forming the desired nickel pincer complex. In other words, an improved synthetic method for *m*-$C_6H_4(OP^tBu_2)(NHP^tBu_2)$ had to be developed.

We first tested the procedures that had been successfully applied to the synthesis of the less bulky POCNP-type proligands (*m*-$C_6H_4(OPPh_2)(NHPPh_2)$ [35] and *m*-$C_6H_4(OP^iPr_2)(NHP^iPr_2)$ [36]), the symmetric POCOP- and PNCNP-type proligands (*m*-$C_6H_4(OP^tBu_2)_2$ [37] and *m*-$C_6H_4(NHP^tBu_2)_2$ [38]), and the analogous pyridine-based ligand (2,6-$C_5H_3N(OP^tBu_2)(NHP^tBu_2)$ [39]). To our disappointment, none of these methods outperformed the original method as far as the purity of *m*-$C_6H_4(OP^tBu_2)(NHP^tBu_2)$ was concerned. It is possible that the doubly deprotonated form of *m*-aminophenol exists as aggregates, whose structures are dependent on the solvent, counterion, and additive. The degree of aggregation in turn could have a profound impact on its nucleophilic substitution reactions with $^tBu_2PCl$. After an extensive optimization of the reaction conditions, we found that it was beneficial to construct the O–P and N–P bonds in a stepwise manner. This strategy, as detailed in Scheme 1, led to the isolation of *m*-$C_6H_4(OP^tBu_2)(NHP^tBu_2)$ in modest yield with high purity (up to 99%).

Cyclometalation of *m*-$C_6H_4(OP^tBu_2)(NHP^tBu_2)$ with $NiCl_2$ was straightforwardly accomplished in the presence of Et_3N under heating (Scheme 2). The desired pincer complex **35-Cl** was isolated as a yellow air-stable solid following purification by column chromatography. Going from the proligand to **35-Cl**, the most notable changes in the NMR spectra are the disappearance of one hydrogen resonance in the aromatic region, the diminished two-bond coupling constant for the NH resonance ($^2J_{H\text{-}P}$: 10.8 → ~0 Hz), and the significantly shifted phosphorus resonances (150.6 → 185.6 ppm for OP^tBu_2; 58.2 → 112.3 ppm for NHP^tBu_2). The $^{31}P\{^1H\}$ NMR spectrum of **35-Cl** features two

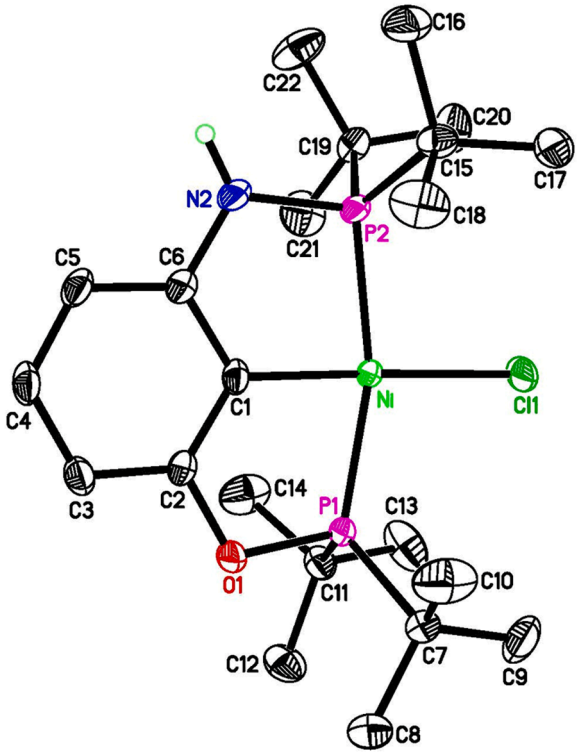

Fig. 3. ORTEP of {2,6-$C_6H_3(OP^tBu_2)(NHP^tBu_2)$}NiCl (**35-Cl**) at the 50% probability level (for clarity, all hydrogen atoms except the one bound to nitrogen are omitted). Selected bond lengths (Å) and angles (°): Ni–C(l) 1.897(2), Ni–Cl(1) 2.2191(6), Ni–P(1) 2.1737(6), Ni–P(2) 2.2148(6), P(1)–O(1) 1.6475 (17), P(2)–N(2) 1.685(2); P(1)–Ni–P(2) 165.11(3), C(1)–Ni–Cl(1) 177.61(8), C (2)–O(1)–P(1) 111.55(14), C(6)–N(2)–P(2) 115.55(16).

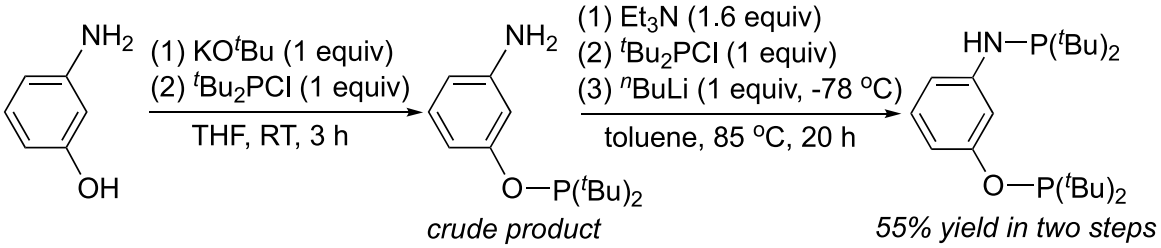

Scheme 1. An improved synthetic route to *m*-$C_6H_4(OP^tBu_2)(NHP^tBu_2)$.

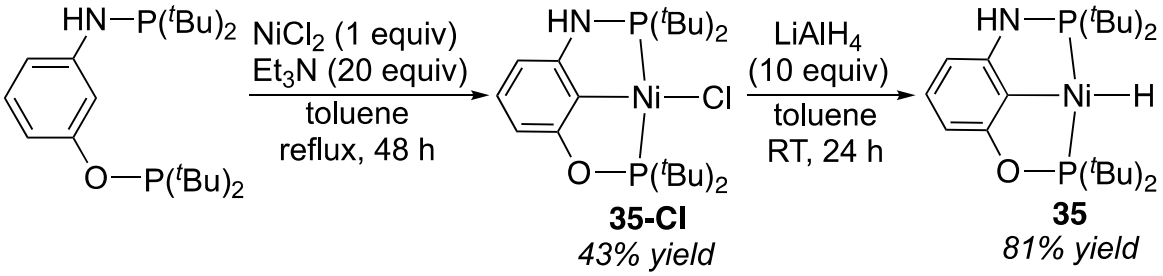

Scheme 2. Synthesis of nickel hydride **35** from *m*-$C_6H_4(OP^tBu_2)(NHP^tBu_2)$.

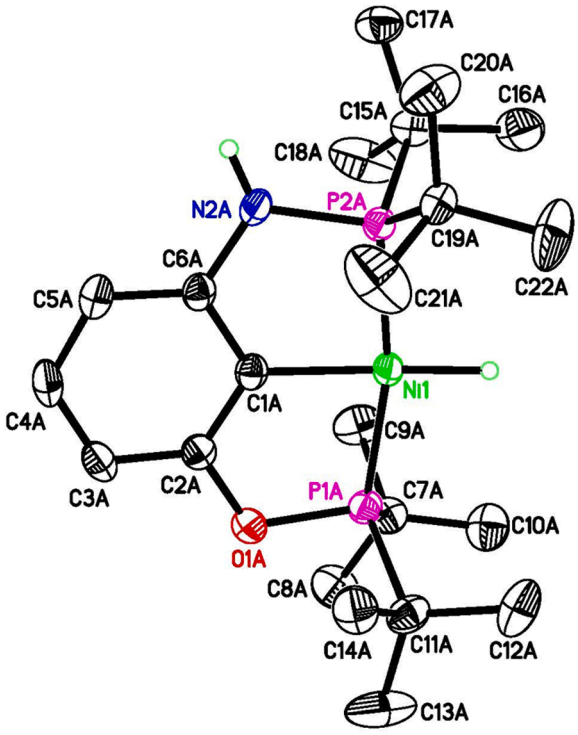

Fig. 4. ORTEP of {2,6-$C_6H_3(OP^tBu_2)(NHP^tBu_2)$}NiH (**35**) at the 50% probability level (for clarity, all hydrogen atoms except those bound to nitrogen and nickel are omitted and only one of the two independent molecules is shown). Selected bond lengths (Å) and angles (°): Ni(1)–H 1.438(3), Ni(1)–C(lA) 1.8993 (19), Ni(1)–P(1A) 2.1094(5), Ni(1)–P(2A) 2.1381(5), P(1A)–O(1A) 1.6662(15), P(2A)–N(2A) 1.6975(17); P(1A)–Ni(1)–P(2A) 167.78(2), C(1A)–Ni(1)–H 178 (1), C(2A)–O(1A)–P(1A) 111.26(12), C(6A)–N(2A)–P(2A) 114.40(13).

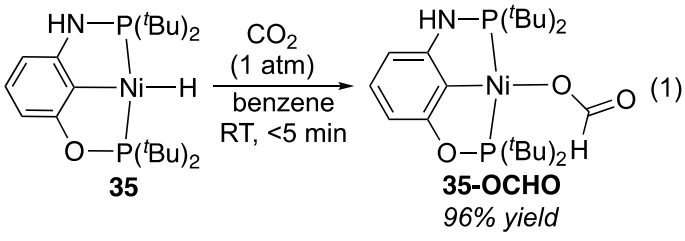

doublets with a large coupling constant of 298 Hz, consistent with a pincer complex that contains two different *trans*-positioned phosphorus donors. The structure of **35-Cl** was more unambiguously established by X-ray crystallography (Fig. 3), which also provided a great opportunity to compare the phosphinite donor (P1) with the phosphinous amide donor (P2) within the same molecule. Evidently, the P1 atom forms a shorter bond with nickel (2.1737(6) Å for Ni–P1 vs 2.2148(6) Å for Ni–P2), implying a stronger interaction between the phosphinite donor and nickel. It is also worth noting that the nitrogen is flat, and the NH group is engaged in a hydrogen-bonding interaction with the chloride from a neighboring molecule of **35-Cl**.

The target nickel hydride **35** was prepared by stirring **35-Cl** with a suspension of $LiAlH_4$ in toluene followed by filtration through Celite (Scheme 2). The isolated product was a pale-yellow powder. The presence of a hydride ligand was confirmed by the proton resonance centered at –8.32 ppm (in C_6D_6) as an apparent triplet ($^2J_{H–P1} = {}^2J_{H–P2} =$ 54.4 Hz) and the medium-intensity IR band found at 1763 cm^{-1}. The hydride was also located crystallographically (Fig. 4). As expected, replacing the chloride with hydride, which is considerably smaller in size, causes contraction of Ni–P bonds by 0.06–0.08 Å. This is also reflected by the phosphorus resonances (doublets at 218.4 and 145.6 ppm), which are shifted downfield relative to the signals of **35-Cl**. Nevertheless, the Ni–P bond formed by the phosphinite donor remains to be the shorter one. While the nitrogen in **35** still adopts the planar geometry, the NH group no longer participates in any hydrogen-bonding interactions.

2.2. Reduction of CO_2

Having made a brand-new nickel hydride, we wished to know if it could react with CO_2. When a solution of **35** in C_6D_6 (73 mM) was exposed to CO_2 (1 atm) at room temperature, it quickly turned slightly darker while forming a yellow precipitate. The NMR spectra of the sample confirmed that **35** was fully consumed and replaced by a new pincer complex. The observation of a broad proton resonance at 8.51 ppm suggested that CO_2 insertion was successful, and the product must be the nickel formate complex (**35-OCHO**). The reaction was then scaled up in a Schlenk flask, allowing the isolation of **35-OCHO** in an almost quantitative yield (eq 1).

To confirm the presence of a formate group, $^{13}C\{^1H\}$ spectrum of **35-OCHO** was recorded. Because **35-OCHO** has a relatively low solubility in C_6D_6 (2.9 mg/mL), $CDCl_3$ was used as the deuterated solvent to

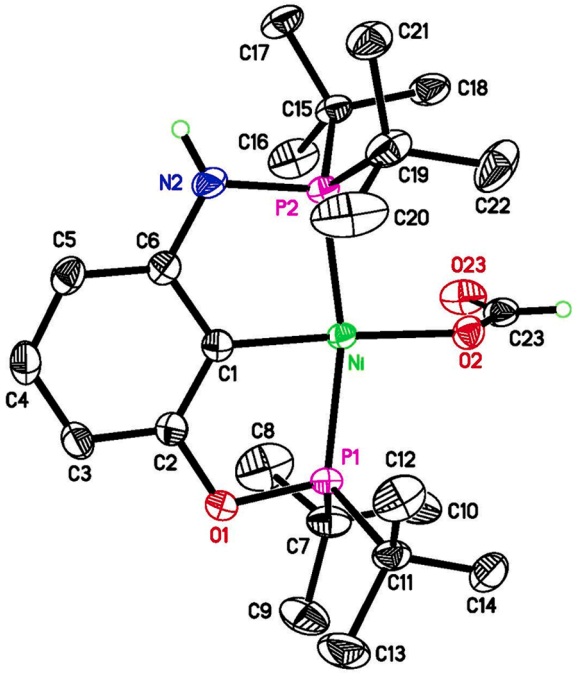

Fig. 5. ORTEP of {2,6-C_6H_3(OP^tBu_2)(NHP^tBu_2)}NiOCHO (**35-OCHO**) at the 50% probability level (for clarity, all hydrogen atoms except the one bound to nitrogen and carbonyl carbon are omitted). Selected bond lengths (Å) and angles (°): Ni–C(1) 1.8966(18), Ni–O(2) 1.9214(13), Ni–P(1) 2.1894(5), Ni–P(2) 2.2245(5), P(1)–O(1) 1.6392(14), P(2)–N(2) 1.6794(17); P(1)–Ni–P(2) 164.300 (19), C(1)–Ni–O(2) 173.43(7), C(2)–O(1)–P(1) 112.29(12), C(6)–N(2)–P(2) 114.92(13).

dissolve the formate complex, which displayed a singlet at 168.6 ppm attributed to the OCHO resonance. Interestingly, the NMR sample left at room temperature overnight was analyzed as a 4 : 1 mixture of **35-OCHO** and **35-Cl**. The halogen exchange process was accelerated at 80 °C, leading to a quantitative conversion of **35-OCHO** to **35-Cl** (along with $CDHCl_2$) in 4 h. This result suggested that de-insertion of CO_2 from **35-OCHO** took place and the resulting hydride **35** underwent halogen exchange with $CDCl_3$. In fact, simply heating a C_6D_6 solution of **35-OCHO** (in a sealed NMR tube) at 80 °C produced a small amount of **35** (<5%). Presumably, the released CO_2 stayed in the headspace. A control experiment also confirmed that **35** dissolved in $CDCl_3$ was fully converted to **35-OCHO** along with $CDHCl_2$ in 2 h.

The structure of **35-OCHO** was further studied by X-ray crystallography (Fig. 5). Upon CO_2 insertion, the Ni–P bonds are elongated to lengths similar to those determined for **35-Cl**. Once again, the phosphinite donor forms a shorter bond with nickel than the phosphinous amide donor (2.1894(5) Å for Ni–P1 vs 2.2245(5) Å for Ni–P2). The formate group adopts an orientation that is perpendicular to the coordination plane, likely to avoid the steric clash with the *tert*-butyl groups. Unsurprisingly, the carbonyl oxygen (O23) forms a hydrogen bond with the NH group of a neighboring molecule. The strengths of the hydrogen bond correlate inversely with the N–H stretching frequencies: **35-OCHO** (3207 cm^{-1}) > **35-Cl** (3354 cm^{-1}) > **35** (3385 cm^{-1}). Furthermore, the N–H band of **35-OCHO** is broad, in contrast to the sharp N–H bands observed with **35-Cl** and **35**.

2.3. Comparison of the three pincer systems

In an attempt to assess the air stability of **35**, its solution in C_6D_6 was intentionally exposed to air, which resulted in direct CO_2 capture to form **35-OCHO**. Powder X-ray diffraction patterns for an air-exposed sample of **35**, however, showed no change after a week, indicating that direct air capture failed to occur on the solid surface. The behavior in solution is nevertheless fascinating, which prompted us to examine if the reactivity is unique to **35**. For a more quantitative comparison, toluene solutions of **13, 21**, and **35** were stirred in air under the same conditions (i.e., 2.2 mM concentration, 21 °C, 360 rpm stirring rate, 396 ppm CO_2 level). The PNCNP pincer complex **21** took the shortest time (3 h) to be fully converted to the corresponding formate complex (**21-OCHO**). The POCNP derivative **35** ranked second, requiring 5 h to complete CO_2 capture. The POCOP pincer complex **13** was the slowest to react; its reaction with CO_2 from the air did not complete until after 26 h.

Next, the relative thermodynamic favorability of CO_2 insertion (ΔΔG) was obtained using the NMR method that we developed earlier [28,30]. As illustrated in Scheme 3, the equilibrium constant (K_{eq}) for the CO_2 exchange reaction between a nickel formate complex and a nickel hydride supported by a different pincer ligand can be measured, provided that CO_2 insertion and de-insertion are kinetically feasible. Because CO_2 insertion is typically fast, the amount of free CO_2 present in the system is often negligible (for experimental evidence, see Section 4.7). A K_{eq} value smaller than 1 means that ΔΔG has a positive value and [Ni]–H reacts with CO_2 more favorably than [Ni']–H. Thus, the measured K_{eq} value of 0.65 ± 0.02 for eq 2 indicates that ΔG for CO_2 insertion is improved by 0.25 kcal/mol when the O linker in **35** is replaced by an NH linker (Scheme 4). Conversely, the measured K_{eq} value of 1.64 ± 0.06 for eq 3 translates to a ΔΔG value of –0.29 kcal/mol or, qualitatively, a thermodynamically less favorable process with the POCOP pincer system.

The results described above clearly establishes the advantage of using NH over O as the linker to build pincer-supported nickel hydrides for CO_2 reduction. A comparison of the bond metrics among the three pincer systems (Table 1) shows that the Ni–C_{ipso} bonds are nearly identical. Importantly, the phosphinous amide donor consistently forms a longer Ni–P bond than the phosphinite donor, whether the comparison is made within the same molecule (**35** or **35-OCHO**) or between molecules (**21** vs **13**, or **21-OCHO** vs **13-OCHO**). This trend has also been observed with other pincer complexes that involve palladium [40] or X-type ligands beyond hydride and formate [41]. Because Ni–P_{NH} bonds are longer than Ni–P_O bonds, the steric approachability of the Ni–H bond follows the decreasing order of **21** (PNCNP) > **35** (POCNP) > **13** (POCOP), which explains the relative rates of CO_2 capture for the three nickel hydrides. The thermodynamic data can be rationalized by the strengths of the Ni–OCHO bonds. The formate group would prefer a harder $[(pincer)Ni]^+$ fragment to increase the electrostatic contribution to the Ni–OCHO bond. Natural population analysis (NPA) and cyclic voltammetry studies have confirmed that the PNCNP pincer system is indeed less electron-rich than the POCOP pincer system [41]. The backbone linkers can alter the electronic property of the pincer ligand not only through the phosphorus donors but also via the ipso carbon (π-donation to the aryl ring) [42]. The less negative NPA charge calculated for the ipso carbon of the PNCNP pincer ligand implies that the diminished π-donation from the NH linkers is mainly responsible for creating a less electron-rich nickel center [41].

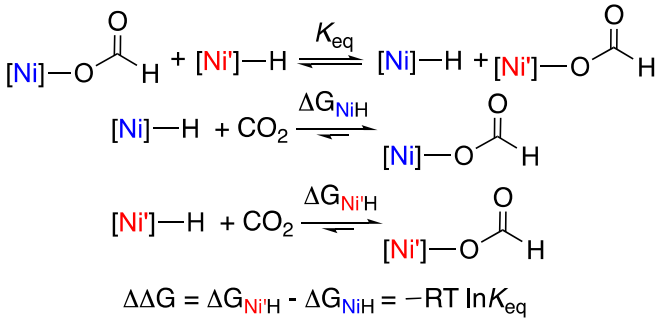

Scheme 3. Method of determining the relative thermodynamic favorability of CO_2 insertion.

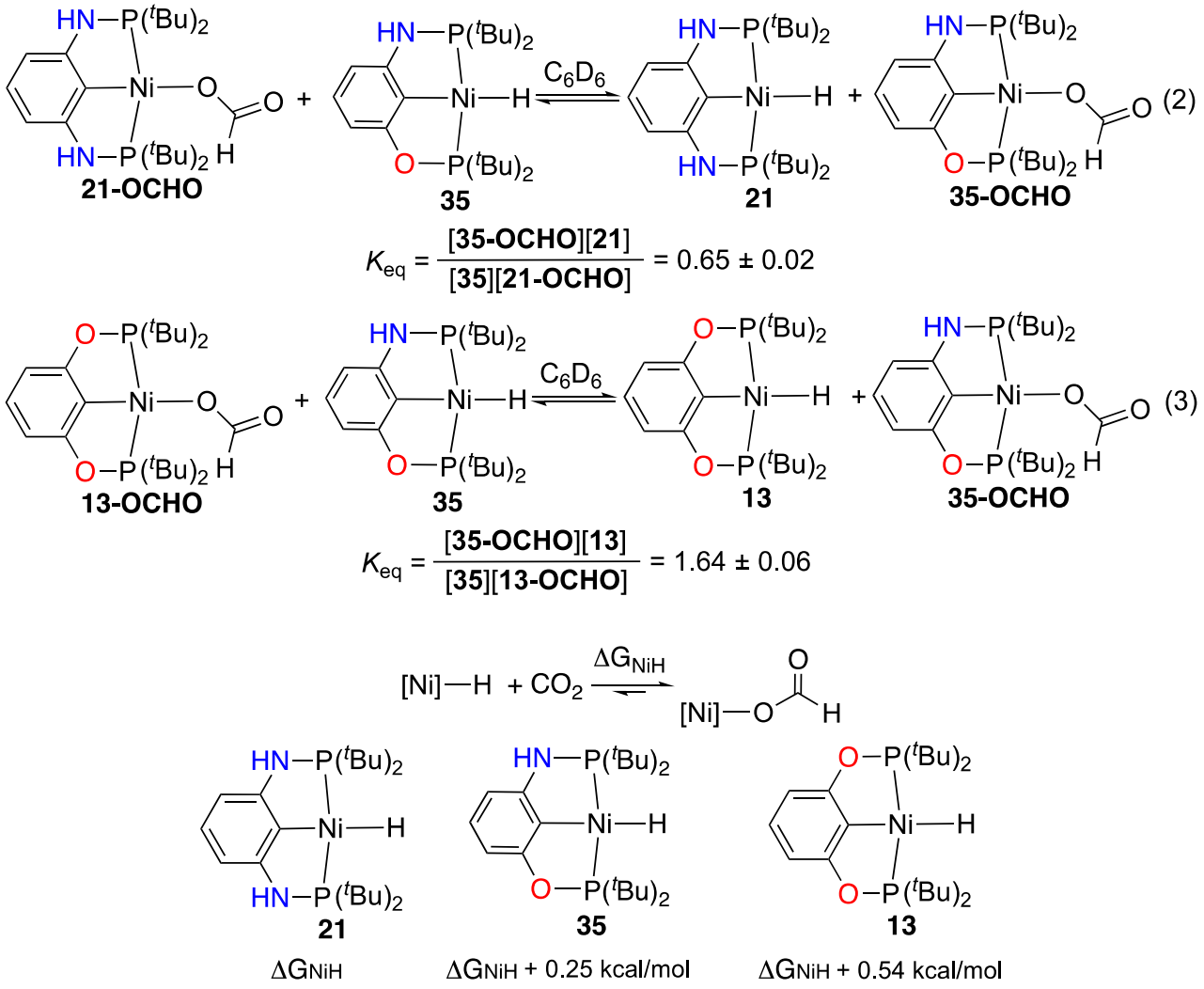

Scheme 4. Relative thermodynamic favorability of CO_2 insertion with the three pincer systems.

Table 1
Comparison of key bond lengths and angles of the hydride and formate complexes.

	Ni–C_{ipso} (Å)	Ni–P_O (Å)	Ni–P_{NH} (Å)	P–Ni–P (°)	reference
13	1.892(3)	2.1160(5)		166.26(3)	33
35[a]	1.8993(19)	2.1094(5)	2.1381(5)	167.78(2)	this work
	1.9019(19)	2.1117(5)	2.1394(5)	167.83(2)	
21	1.9086(18)		2.1270(6), 2.1326(6)	169.79(2)	18
13-OCHO	1.886(2)	2.2040(7), 2.1817(8)		164.02(3)	11
35-OCHO	1.8966(18)	2.1894(5)	2.2245(5)	164.300(19)	this work
21-OCHO	1.908(2)		2.2147(6), 2.2333(6)	165.31(3)	18

[a] **35** crystallized with two independent molecules, hence two sets of data.

3. Conclusions

We have successfully improved the synthetic method for *m*-$C_6H_4(OP^tBu_2)(NHP^tBu_2)$, a hybrid pincer-type proligand that was needed to build the POCNP-pincer ligated nickel hydride complex. This has provided us with the opportunity to systematically study the effect of the backbone linker (O vs NH) on the reactivity of the nickel hydrides in the context of CO_2 reduction. The comparative study has shown that the rates for CO_2 capture from air follow the decreasing order PNCNP > POCNP > POCOP. For the thermodynamic favorability of CO_2 insertion, the PNCNP pincer system also ranks first, followed by the POCNP pincer system and then the POCOP pincer system. The kinetic preference for the PNCNP pincer system can be attributed to the more exposed Ni–H bond created by the relatively longer Ni–P_{NH} bonds. The thermodynamic advantage can be explained by a stronger Ni–OCHO bond formed by the PNCNP pincer ligand, which is less electron rich than the POCOP pincer ligand.

4. Experimental

4.1. Materials and methods

Unless otherwise noted, all compounds were prepared and handled under an argon atmosphere using standard glovebox and Schlenk techniques. Dry and oxygen-free toluene and pentane used for the syntheses were collected from an Innovative Technology solvent

purification system. Anhydrous and inhibitor-free tetrahydrofuran (THF) was purchased from Sigma-Aldrich (packed in a Sure/Seal™ bottle). Dichloromethane (CH_2Cl_2) and pentane used for column chromatography and recrystallization were purchased from Fisher Scientific. Chloroform-*d* (99.8% D, 0.03% v/v tetramethylsilane) was purchased from Cambridge Isotope Laboratories. These commercial reagents were used as received without further purification. Benzene-d_6 (99.5% D) and benzene were dried over sodium-benzophenone and then distilled under agon. Triethylamine was dried over calcium hydride prior to distillation under argon. Complexes **13** [33], **13-OCHO** [11], **21** [18] and **21-OCHO** [18] were prepared as described in the literature. NMR spectra were recorded at 23 °C on a Bruker AV400 or NEO400 NMR spectrometer. The chemical shift values for ^{1}H and ^{13}C{^{1}H} NMR spectra were referenced internally to the residual solvent resonances or tetramethylsilane (0 ppm). ^{31}P{^{1}H} NMR spectra were referenced externally to 85% phosphoric acid (0 ppm). IR spectra were recorded on a PerkinElmer Spectrum Two Fourier transform infrared spectrometer equipped with a Smart Orbit diamond attenuated-total-reflectance (ATR) accessory. The CO_2 level in the fume hood was measured by a Cole-Parmer data logging carbon dioxide monitor (item # EW-94560–00). Finely-ground powdered samples of **35** and **35-OCHO** were analyzed at room temperature using Cu Kα radiation (3–100 deg in θ-2θ, 2 deg/min, 0.01 deg step width, reflection mode) on a Rigaku MiniFlex 6 G diffractometer.

4.2. Synthesis of *m*-$C_6H_4(OP^tBu_2)(NHP^tBu_2)$

This compound was previously reported by Liu and co-workers, although its purity was low (~50%) [34]. The procedure described here provided samples with higher purity (up to 99%). Under an argon atmosphere, *m*-aminophenol (1.60 g, 14.7 mmol) was mixed with 40 mL of THF in a 100 mL Schlenk flask, after which potassium *tert*-butoxide (1.65 g, 14.7 mmol) and di-*tert*-butylchlorophosphine (2.65 g, 14.7 mmol) were added sequentially. The resulting mixture was stirred at room temperature for 3 h and then concentrated under vacuum to yield *m*-$C_6H_4(OP^tBu_2)(NH_2)$ (along with KCl, the presumed by-product) as a brown oil. ^{1}H NMR (400 MHz, C_6D_6): δ 6.99 (t, $^3J_{H\text{-}H}$ = 8.0 Hz, Ar*H*, 1H), 6.81 (dt, $^3J_{H\text{-}H}$ = 8.0 Hz, ^4J = 2.2 Hz, Ar*H*, 1H), 6.54 (q, $^4J_{H\text{-}P}$ = $^4J_{H\text{-}H}$ = 2.2 Hz, Ar*H*, 1H), 6.02 (dd, $^3J_{H\text{-}H}$ = 8.0 Hz, $^4J_{H\text{-}H}$ = 2.0 Hz, Ar*H*, 1H), 2.80 (s, NH_2, 2H), 1.15 (d, $^3J_{H\text{-}P}$ = 11.6 Hz, C(CH_3)$_3$, 18H). ^{31}P{^{1}H} NMR (162 MHz, C_6D_6): δ 149.9 (s, OP^tBu_2).

In the second step of the synthesis, the newly formed phosphinite was treated with 40 mL of toluene, followed by the addition of triethylamine (2.37 g, 23.4 mmol) and di-*tert*-butylchlorophosphine (2.65 g, 14.7 mmol). The reaction flask was subsequently chilled in a dry ice/acetone bath (–78°C) prior to slow addition of an *n*-butyllithium solution (1.6 M in hexanes, 9.2 mL, 14.7 mmol, added over 30 min via a syringe pump). The resulting mixture was warmed to room temperature and then heated at 85°C for 20 h. After cooling, the volatiles were removed under vacuum. The residue was extracted with pentane (15 mL × 5) and filtered through a short pad of Celite. The resulting filtrate was placed under vacuum for an extended period of time (5 h), giving the desired product as a viscous brown oil (3.20 g, 55% yield). ^{1}H NMR (400 MHz, C_6D_6): δ 7.29 (quint, $^4J_{H\text{-}P}$ = $^4J_{H\text{-}H}$ = 2.4 Hz, Ar*H*, 1H), 7.08 (t, $^3J_{H\text{-}H}$ = 8.0 Hz, Ar*H*, 1H), 6.88 (dt, $^3J_{H\text{-}H}$ = 8.0 Hz, ^4J = 2.4 Hz, Ar*H*, 1H), 6.70 (dt, $^3J_{H\text{-}H}$ = 8.0 Hz, ^4J = 2.4 Hz, Ar*H*, 1H), 3.82 (d, $^2J_{H\text{-}P}$ = 10.8 Hz, N*H*, 1H), 1.16 (d, $^3J_{H\text{-}P}$ = 12.0 Hz, C(CH_3)$_3$, 18H), 0.99 (d, $^3J_{H\text{-}P}$ = 11.6 Hz, C(CH_3)$_3$, 18H). ^{31}P{^{1}H} NMR (162 MHz, C_6D_6): δ 150.6 (s, OP^tBu_2, 1P), 58.2 (s, HNP^tBu_2, 1P).

4.3. Synthesis of {2,6-$C_6H_3(OP^tBu_2)(NHP^tBu_2)$}NiCl (**35-Cl**)

To a 100 mL Schlenk flask were added anhydrous nickel chloride (587 mg, 4.53 mmol), *m*-$C_6H_4(OP^tBu_2)(NHP^tBu_2)$ (1.80 g, 4.53 mmol), triethylamine (9.17 g, 90.6 mmol), and toluene (30 mL). The resulting mixture was refluxed under argon for 48 h. After cooling, the volatiles were removed under vacuum. The residue was exposed to air, washed with pentane (10 mL), and subject to further purification by column chromatography (eluted with 1:9 CH_2Cl_2-pentane first, followed by 1:1 CH_2Cl_2-pentane). The desired product was isolated as a yellow solid (948 mg, 43% yield). X-ray-quality crystals were grown at room temperature from CH_2Cl_2-pentane (1:1). ^{1}H NMR (400 MHz, $CDCl_3$): δ 6.81 (t, $^3J_{H\text{-}H}$ = 7.6 Hz, Ar*H*, 1H), 6.19 (d, $^3J_{H\text{-}H}$ = 8.0 Hz, Ar*H*, 1H), 6.13 (d, $^3J_{H\text{-}H}$ = 8.0 Hz, Ar*H*, 1H), 4.13 (s, N*H*, 1H), 1.50 (d, $^3J_{H\text{-}P}$ = 11.6 Hz, C(CH_3)$_3$, 18H), 1.47 (d, $^3J_{H\text{-}P}$ = 11.2 Hz, C(CH_3)$_3$, 18H). ^{13}C{^{1}H} NMR (101 MHz, $CDCl_3$): δ 169.7 (dd, $J_{C\text{-}P}$ = 13.3 and 5.8 Hz, ArC_{ortho}), 160.2 (dd, $J_{C\text{-}P}$ = 23.9 and 4.9 Hz, ArC_{ortho}), 127.7 (s, ArC_{para}), 121.3 (dd, $^2J_{C\text{-}P}$ = 21.9 and 19.0 Hz, ArC_{ipso}), 102.8 (d, $^3J_{C\text{-}P}$ = 13.6 Hz, ArC_{meta}), 102.3 (d, $^3J_{C\text{-}P}$ = 13.3 Hz, ArC_{meta}), 39.2 (dd, $J_{C\text{-}P}$ = 10.6 and 3.9 Hz, *C*(CH$_3$)$_3$), 37.8 (dd, $J_{C\text{-}P}$ = 12.9 and 2.8 Hz, *C*(CH$_3$)$_3$), 28.4 (d, $^2J_{C\text{-}P}$ = 4.9 Hz, C(*C*H$_3$)$_3$), 28.2 (d, $^2J_{C\text{-}P}$ = 4.8 Hz, C(*C*H$_3$)$_3$). ^{31}P{^{1}H} NMR (162 MHz, $CDCl_3$): δ 185.6 (d, $^2J_{P\text{-}P}$ = 298 Hz, OP^tBu_2, 1P), 112.3 (d, $^2J_{P\text{-}P}$ = 298 Hz, HNP^tBu_2, 1P). Selected ATR-IR data (solid, cm^{-1}): 3354 ($\nu_{N–H}$), 2968, 2946, 2898, 2866, 1575, 1471, 1442, 1370, 1352, 1293, 1213, 1178. Anal. Calcd for $C_{22}H_{40}NOP_2ClNi$: C, 53.85; H, 8.22; N, 2.85; Cl, 7.23. Found: C, 53.84; H, 8.22; N, 2.83; Cl, 7.34.

4.4. Synthesis of {2,6-$C_6H_3(OP^tBu_2)(NHP^tBu_2)$}NiH (**35**)

To a 25 mL Schlenk flask were added {2,6-$C_6H_3(OP^tBu_2)(NHP^tBu_2)$} NiCl (530 mg, 1.08 mmol), lithium aluminum hydride (409 mg, 10.8 mmol), and toluene (6 mL). The resulting suspension was stirred under argon for 24 h and then filtered through a pad of Celite. The filtrate was pumped to dryness, giving the desired product as a pale-yellow powder (400 mg, 81% yield). X-ray-quality crystals were obtained from slow evaporation of a solution of **35** in C_6D_6. ^{1}H NMR (400 MHz, C_6D_6): δ 7.08 (t, $^3J_{H\text{-}H}$ = 7.6 Hz, Ar*H*, 1H), 6.81 (d, $^3J_{H\text{-}H}$ = 8.0 Hz, Ar*H*, 1H), 6.37 (d, $^3J_{H\text{-}H}$ = 7.6 Hz, Ar*H*, 1H), 3.94 (s, N*H*, 1H), 1.36 (d, $^3J_{H\text{-}P}$ = 13.6 Hz, C(CH_3)$_3$, 18H), 1.19 (d, $^3J_{H\text{-}P}$ = 13.6 Hz, C(CH_3)$_3$, 18H), –8.32 (t, $^2J_{H\text{-}P1}$ = $^2J_{H\text{-}P2}$ = 54.4 Hz, Ni*H*, 1H). ^{13}C{^{1}H} NMR (101 MHz, C_6D_6): δ 169.2 (dd, $J_{C\text{-}P}$ = 13.1 and 6.2 Hz, ArC_{ortho}), 159.8 (dd, $J_{C\text{-}P}$ = 24.0 and 4.9 Hz, ArC_{ortho}), 140.9 (dd, $^2J_{C\text{-}P}$ = 17.0 and 14.3 Hz, ArC_{ipso}), 128.0 (s, Ar*C*-$_{para}$), 102.9 (d, $^3J_{C\text{-}P}$ = 13.7 Hz, ArC_{meta}), 102.6 (d, $^3J_{C\text{-}P}$ = 13.3 Hz, ArC_{meta}), 37.8 (dd, $J_{C\text{-}P}$ = 14.8 and 3.6 Hz, *C*(CH$_3$)$_3$), 36.4 (dd, $J_{C\text{-}P}$ = 16.7 and 2.5 Hz, *C*(CH$_3$)$_3$), 28.9 (d, $^2J_{C\text{-}P}$ = 6.3 Hz, C(*C*H$_3$)$_3$), 28.7 (d, $^2J_{C\text{-}P}$ = 6.3 Hz, C(*C*H$_3$)$_3$). ^{31}P{^{1}H} NMR (162 MHz, C_6D_6): δ 218.4 (d, $^2J_{P\text{-}P}$ = 261 Hz, OP^tBu_2, 1P), 145.6 (d, $^2J_{P\text{-}P}$ = 261 Hz, HNP^tBu_2, 1P). Selected ATR-IR data (solid, cm^{-1}): 3385 ($\nu_{N–H}$), 2957, 2942, 2895, 1763 ($\nu_{Ni–H}$), 1566, 1473, 1439, 1369, 1346, 1195. Anal. Calcd for $C_{22}H_{41}NOP_2Ni$: C, 57.92; H, 9.06; N, 3.07. Found: C, 57.68; H, 8.90; N, 3.07.

4.5. Synthesis of {2,6-$C_6H_3(OP^tBu_2)(NHP^tBu_2)$}NiOCHO (**35-OCHO**)

Under an argon atmosphere, nickel hydride **35** (200 mg, 0.44 mmol) was mixed with benzene (10 mL) in a 25 mL Schlenk flask. The resulting solution was degassed via three freeze-pump-thaw cycles and then exposed to CO_2 (1 atm, 23 °C), which resulted in a slight darkening of the solution followed by the formation of a yellow precipitate. The reaction mixture was stirred for another 2 min before being placed under vacuum. The desired formate complex was isolated as a yellow solid (210 mg, 96% yield). X-ray-quality crystals were obtained from a solution of **35-OCHO** in CH_2Cl_2 layered with pentane. ^{1}H NMR (400 MHz, $CDCl_3$): δ 8.16 (s, OC*H*O, 1H), 6.78 (t, $^3J_{H\text{-}H}$ = 7.6 Hz, Ar*H*, 1H), 6.13 (d, $^3J_{H\text{-}H}$ = 8.0 Hz, Ar*H*, 1H), 6.08 (d, $^3J_{H\text{-}H}$ = 7.6 Hz, Ar*H*, 1H), 4.22 (s, N*H*, 1H), 1.47 (d, $^3J_{H\text{-}P}$ = 9.6 Hz, C(CH_3)$_3$, 18H), 1.44 (d, $^3J_{H\text{-}P}$ = 9.2 Hz, C(CH_3)$_3$, 18H). ^{1}H NMR (400 MHz, C_6D_6): δ 8.51 (br, OC*H*O, 1H), 6.89 (t, $^3J_{H\text{-}H}$ = 7.6 Hz, Ar*H*, 1H), 6.44 (d, $^3J_{H\text{-}H}$ = 8.0 Hz, Ar*H*, 1H), 5.99 (d, $^3J_{H\text{-}H}$ = 7.6 Hz, Ar*H*, 1H), 3.71 (s, N*H*, 1H), 1.46 (d, $^3J_{H\text{-}P}$ = 14.0 Hz, C(CH_3)$_3$, 18H), 1.29 (d, $^3J_{H\text{-}P}$ = 13.6 Hz, C(CH_3)$_3$, 18H); sometimes the OC*H*O resonance was resolved as a triplet ($^4J_{H\text{-}P}$ = 2.4 Hz). ^{13}C{^{1}H} NMR (101 MHz, $CDCl_3$): δ 169.9 (dd, $J_{C\text{-}P}$ = 11.1 and 5.6 Hz, ArC_{ortho}), 168.6 (s, O*C*HO), 160.4 (dd, $J_{C\text{-}P}$ = 23.2 and 5.1 Hz, ArC_{ortho}), 127.8 (s, ArC_{para}), 116.4 (dd, $^2J_{C\text{-}P}$ = 21.2 and 19.2 Hz, ArC_{ipso}), 102.9 (d, $^3J_{C\text{-}P}$ =

14.1 Hz, ArC_{meta}), 102.4 (d, $^{3}J_{C\text{-}P}$ = 13.1 Hz, ArC_{meta}), 38.8 (dd, $J_{C\text{-}P}$ = 10.6 and 3.5 Hz, $C(CH_3)_3$), 37.5 (dd, $J_{C\text{-}P}$ = 12.6 and 2.5 Hz, $C(CH_3)_3$), 28.2 (d, $^{2}J_{C\text{-}P}$ = 6.1 Hz, C(CH_3)$_3$), 27.7 (d, $^{2}J_{C\text{-}P}$ = 5.1 Hz, C(CH_3)$_3$). ^{31}P{^{1}H} NMR (162 MHz, $CDCl_3$): δ 185.3 (d, $^{2}J_{P\text{-}P}$ = 273 Hz, OP^{t}Bu$_2$, 1P), 111.7 (d, $^{2}J_{P\text{-}P}$ = 273 Hz, HNP^{t}Bu$_2$, 1P). ^{31}P{^{1}H} NMR (162 MHz, C_6D_6): δ 185.2 (d, $^{2}J_{P\text{-}P}$ = 276 Hz, OP^{t}Bu$_2$, 1P), 111.7 (d, $^{2}J_{P\text{-}P}$ = 276 Hz, HNP^{t}Bu$_2$, 1P). Selected ATR-IR data (solid, cm^{-1}): 3207 ($\nu_{N\text{–}H}$), 2962, 2949, 2897, 2867, 1607 (ν_{OCO}), 1577, 1472, 1445, 1366, 1335, 1216, 1131, 1124, 1006. Anal. Calcd for $C_{23}H_{41}NO_3P_2Ni$: C, 55.23; H, 8.26; N, 2.80. Found: C, 55.24; H, 8.30; N, 2.80.

4.6. CO_2 capture by nickel hydrides

To three separate 20 mL scintillation vials equipped with a stir bar (8 × 12.7 mm) were added a different nickel hydride complex (**13**/**21**/**35**, 5.0 mg, 11 μmol) and toluene (5.0 mL). The resulting solutions were stirred at the same speed (360 rpm) in a fume hood with a CO_2 level of 396 ppm and an ambient temperature of 21 °C. The progress of CO_2 capture was monitored by periodically withdrawing aliquots from the solutions for ^{31}P{^{1}H} NMR analyses. Each experiment was continued until full conversion of the nickel hydride was achieved.

4.7. Determination of equilibrium constants

Under an argon atmosphere, a nickel hydride (2 mg), a nickel formate supported by a different pincer ligand (2 mg), and C_6D_6 (0.6 mL) were mixed in a J. Young NMR tube and then sealed. The CO_2 exchange reaction was monitored by ^{1}H and ^{31}P{^{1}H} NMR spectroscopy at room temperature (21 °C) for a week, although the equilibrium usually was established after a day. The experiment was repeated, and the equilibrium was approached from both directions. The equilibrium constants were calculated based on the NMR integrations of the NiH and NiOCHO resonances. The reported values are the averages of four data sets (two for each direction). To rule out the possibility that free CO_2 may be present in the system, one of the K_{eq} measurements (**35-OCHO** mixed with **21**) was repeated by doubling the volume of C_6D_6 to 1.2 mL (i.e., changing the headspace-to-solution volume ratio). This resulted in no change to the K_{eq} value. In addition, at room temperature, the release of CO_2 from **35-OCHO** (in C_6D_6) to give **35** was not observed after 5 days.

4.8. X-ray crystallography

Crystal data collection and refinement parameters are provided in the supplementary material. The intensity data were collected at 150 K on a Bruker D8 Venture Photon-II diffractometer using Mo Kα radiation, λ = 0.71073 Å. The data frames were processed using the program SAINT. The data were corrected for decay, Lorentz, and polarization effects as well as absorption and beam corrections. The structures were solved by a combination of direct methods and the difference Fourier technique as implemented in the SHELX suite of programs and refined by full-matrix least squares on F^2 for reflections out to 0.75 Å. Non-hydrogen atoms were refined with anisotropic displacement parameters. The hydride in **35** was located directly from the difference map for both independent molecules; the coordinates and isotropic displacement parameters were refined. Hydrogen atoms bound to the nitrogen atoms were located directly from the difference map and treated with a riding model. All remaining hydrogen atoms were calculated and treated with a riding model. The isotropic displacement parameters were defined as a*Ueq (a = 1.5 for methyl, 1.2 for all others) of the adjacent atom. Crystals of **35** are pseudo-merohedrally twinned, twin law applied 1 0 0 0 -1 0 0 0 -1. Crystal structures of **35-Cl, 35**, and **35-OCHO** were deposited at the Cambridge Crystallographic Data Centre (CCDC) and assigned the deposition numbers CCDC 2377135 – 2377137.

CRediT authorship contribution statement

Mahmood Ahmadianpoor: Writing – original draft, Investigation, Formal analysis, Data curation. **Patrick D. Pridemore:** Investigation, Formal analysis. **Jeanette A. Krause:** Writing – review & editing, Investigation, Formal analysis, Data curation. **Hairong Guan:** Writing – review & editing, Supervision, Project administration, Funding acquisition, Formal analysis, Data curation, Conceptualization.

Declaration of competing interest

The authors declare that they have no known competing financial interests or personal relationships that could have appeared to influence the work reported in this paper.

Data availability

Data will be made available on request.

Acknowledgements

We thank the U.S. National Science Foundation (NSF) Chemical Catalysis Program (CHE-2102192) and the REU Program (CHE-1950244) for support of this research project and the NSF MRI Program for support of the instrumentation used in this study, which includes a Bruker D8 Venture diffractometer (CHE-1625737) and a Bruker NEO400 MHz NMR spectrometer (CHE-1726092). Funding from the University of Cincinnati is acknowledged for the Rigaku MiniFlex 6 G powder diffractometer.

Supplementary materials

Supplementary material associated with this article can be found, in the online version, at doi:10.1016/j.jorganchem.2024.123399.

References

[1] H. Arakawa, M. Aresta, J.N. Armor, M.A. Barteau, E.J. Beckman, A.T. Bell, J. E. Bercaw, C. Creutz, E. Dinjus, D.A. Dixon, K. Domen, D.L. DuBois, J. Eckert, E. Fujita, D.H. Gibson, W.A. Goddard, D.W. Goodman, J. Keller, G.J. Kubas, H. H. Kung, J.E. Lyons, L.E. Manzer, T.J. Marks, K. Morokuma, K.M. Nicholas, R. Periana, L. Que, J. Rostrup-Nielson, W.M.H. Sachtler, L.D. Schmidt, A. Sen, G. A. Somorjai, P.C. Stair, B.R. Stults, W. Tumas, Catalysis research of relevance to carbon management: progress, challenges, and opportunities, Chem. Rev. 101 (2001) 953–996, https://doi.org/10.1021/cr000018s.

[2] M. Aresta, A. Dibenedetto, Utilisation of CO_2 as a chemical feedstock: opportunities and challenges, Dalton Trans. (2007) 2975–2992, https://doi.org/10.1039/B700658F.

[3] M. Aresta, A. Dibenedetto, A. Angelini, Catalysis for the valorization of exhaust carbon: from CO_2 to chemicals, materials, and fuels. technological use of CO_2, Chem. Rev. 114 (2014) 1709–1742, https://doi.org/10.1021/cr4002758.

[4] N.A. Eberhardt, H. Guan, Nickel hydride complexes, Chem. Rev. 116 (2016) 8373–8426, https://doi.org/10.1021/acs.chemrev.6b00259.

[5] N. Hazari, J.E. Heimann, Carbon dioxide insertion into group 9 and 10 metal-element σ bonds, Inorg. Chem. 56 (2017) 13655–13678, https://doi.org/10.1021/acs.inorgchem.7b02315.

[6] M.Y. Darensbourg, M. Ludwig, C.G. Riordan, Spectroscopic and chemical studies of nickel(II) hydrides, Inorg. Chem. 28 (1989) 1630–1634, https://doi.org/10.1021/ic00308a007.

[7] D.J. Darensbourg, M.Y. Darensbourg, L.Y. Goh, M. Ludvig, P. Wiegreffe, The reaction of $(Cy_3P)_2Ni(H)(CH_3)$ with carbon dioxide. formation of a hydridonickel formate complex, $HNi(O_2CH)(Cy_3P)_2$, J. Am. Chem. Soc. 109 (1987) 7539–7540, https://doi.org/10.1021/ja00258a053.

[8] M. Aresta, E. Quaranta, A. Dibenedetto, P. Giannoccaro, I. Tommasi, M. Lanfranchi, A. Tiripicchio, Oxidative addition of ammonium and iminium tetraphenylborates to low-valent metal complexes. Evidence of selective N–C and N–H activation. A new, easy route to cationic Allyl- and hydridonickel complexes, Organometallics 16 (1997) 834–841, https://doi.org/10.1021/om960602k.

[9] A.J.M. Miller, J.A. Labinger, J.E. Bercaw, Trialkylborane-assisted CO_2 reduction by late transition metal hydrides, Organometallics 30 (2011) 4308–4314, https://doi.org/10.1021/om200364w.

[10] J.A. Zurakowski, M. Bhattacharyya, D.M. Spasyuk, M.W. Drover, Octaboraneyl [Ni(H)(diphosphine)$_2$]$^{+}$ complexes: exploiting phosphine ligand lability for hydride

transfer to an $[NAD]^+$ model, Inorg. Chem. 60 (2021) 37–41, https://doi.org/10.1021/acs.inorgchem.0c03409.
[11] S. Chakraborty, J. Zhang, J.A. Krause, H. Guan, An efficient nickel catalyst for the reduction of carbon dioxide with a borane, J. Am. Chem. Soc. 132 (2010) 8872–8873, https://doi.org/10.1021/ja103982t.
[12] S. Chakraborty, Y.J. Patel, J.A. Krause, H. Guan, Catalytic properties of nickel Bis (phosphinite) pincer complexes in the reduction of CO_2 to methanol derivatives, Polyhedron 32 (2012) 30–34, https://doi.org/10.1016/j.poly.2011.04.030.
[13] K.J. Jonasson, O.F. Wendt, Synthesis and characterization of a family of POCOP pincer complexes with nickel: reactivity towards CO_2 and phenylacetylene, Chem. Eur. J. 20 (2014) 11894–11902, https://doi.org/10.1002/chem.201403246.
[14] T.J. Schmeier, N. Hazari, C.D. Incarvito, J.A. Raskatov, Exploring the reactions of CO_2 with PCP supported nickel complexes, Chem. Commun. 47 (2011) 1824–1826, https://doi.org/10.1039/c0cc03898a.
[15] H.W. Suh, T.J. Schmeier, N. Hazari, R.A. Kemp, M.K. Takase, Experimental and computational studies of the reaction of carbon dioxide with pincer-supported nickel and palladium hydrides, Organometallics 31 (2012) 8225–8236, https://doi.org/10.1021/om3008597.
[16] J.E. Heimann, W.H. Bernskoetter, N. Hazari, J.M. Mayer, Acceleration of CO_2 insertion into metal hydrides: ligand, lewis acid, and solvent effects on reaction kinetics, Chem. Sci. 9 (2018) 6629–6638, https://doi.org/10.1039/c8sc02535e.
[17] S. Murugesan, B. Stöger, M. Weil, L.F. Veiros, K. Kirchner, Synthesis, structure, and reactivity of Co(II) and Ni(II) PCP pincer borohydride complexes, Organometallics 34 (2015) 1364–1372, https://doi.org/10.1021/acs.organomet.5b00075.
[18] J. Chang, J.X. Mao, M. Ding, J. Zhang, X. Chen, Evaluating the catalytic activities of PNCNP pincer group 10 metal hydride complexes: Pd-catalyzed reduction of CO_2 to the formic acid level with $NH_3{\bullet}BH_3$ and $NaBH_4$ under ambient conditions, Inorg. Chem. 62 (2023) 4971–4979, https://doi.org/10.1021/acs.inorgchem.3c00077.
[19] P. Ríos, N. Curado, J. López-Serrano, A. Rodríguez, Selective reduction of carbon dioxide to Bis(silyl)acetal catalyzed by a PBP-supported nickel complex, Chem. Commun. 52 (2016) 2114–2117, https://doi.org/10.1039/c5cc09650b.
[20] G.T. Venkanna, S. Tammineni, H.D. Arman, Z.J. Tonzetich, Synthesis, characterization, and catalytic activity of nickel(II) alkyl complexes supported by pyrrole-diphosphine ligands, Organometallics 32 (2013) 4656–4663, https://doi.org/10.1021/om400630q.
[21] M. Kreye, M. Freytag, P.G. Jones, P.G. Williard, W.H. Bernskoetter, M.D. Walter, Homolytic H_2 cleavage by a mercury-bridged Ni(I) pincer complex [{(PNP)Ni}$_2${μ-Hg}], Chem. Commun. 51 (2015) 2946–2949, https://doi.org/10.1039/c4cc09743b.
[22] C. Yoo, J. Kim, Y. Lee, Synthesis and reactivity of nickel(II) Hydroxycarbonyl species, NiCOOH-κC, Organometallics 32 (2013) 7195–7203, https://doi.org/10.1021/om400881j.
[23] F. Schneck, J. Ahrens, M. Finger, A.C. Stückl, C. Würtele, D. Schwarzer, S. Schneider, The elusive abnormal CO_2 insertion enabled by metal-ligand cooperative photochemical selectivity inversion, Nat. Commun. 9 (2018) 1161, https://doi.org/10.1038/s41467-018-03239-3.
[24] S. Lapointe, E. Khaskin, R.R. Fayzullin, J.R. Khusnutdinova, Nickel(II) complexes with electron-rich, sterically hindered PNP pincer ligands enable uncommon modes of ligand dearomatization, Organometallics 38 (2019) 4433–4447, https://doi.org/10.1021/acs.organomet.9b00558.
[25] H. Li, T.P. Gonçalves, J. Hu, Q. Zhao, D. Gong, Z. Lai, Z. Wang, J. Zheng, K. W. Huang, A pseudodearomatized PN^3P^*Ni–H complex as a ligand and σ-Nucleophilic catalyst, J. Org. Chem. 83 (2018) 14969–14977, https://doi.org/10.1021/acs.joc.8b02205.
[26] H. Li, T.P. Gonçalves, Q. Zhao, D. Gong, Z. Lai, Z. Wang, J. Zheng, K.W. Huang, Diverse catalytic reactivity of a Dearomatized PN^3P^*–nickel hydride pincer complex towards CO_2 reduction, Chem. Commun. 54 (2018) 11395–11398, https://doi.org/10.1039/c8cc05948a.
[27] M.F. Laird, M. Pink, N.P. Tsvetkov, H. Fan, K.G. Caulton, Unusual selectivity of a (Pincer)Ni-hydride reacting with CO_2, Dalton Trans. (2009) 1283–1285, https://doi.org/10.1039/b822677f.
[28] N.P.N. Wellala, H.T. Dong, J.A. Krause, H. Guan, Janus POCOP pincer complexes of nickel, Organometallics 37 (2018) 4031–4039, https://doi.org/10.1021/acs.organomet.8b00619.
[29] R.C. Cammarota, M.V. Vollmer, J. Xie, J. Ye, J.C. Linehan, S.A. Burgess, A. M. Appel, L. Gagliardi, C.C. Lu, A bimetallic nickel-gallium complex catalyzes CO_2 hydrogenation via the intermediacy of an anionic d^{10} Nickel hydride, J. Am. Chem. Soc. 139 (2017) 14244–14250, https://doi.org/10.1021/jacs.7b07911.
[30] N.A. Eberhardt, Synthesis and Reactivity of Nickel POCOP Pincer Complexes for the Reduction of Carbon Dioxide and Related Compounds, Doctoral Dissertation, University of Cincinnati, 2017.
[31] A.J. Nawara-Hultzsch, J.D. Hackenberg, B. Punji, C. Supplee, T.J. Emge, B. C. Bailey, R.R. Schrock, M. Brookhart, A.S. Goldman, Rational design of highly active "hybrid" phosphine-phosphinite iridium pincer catalysts for alkane metathesis, ACS Catal. 3 (2013) 2505–2514, https://doi.org/10.1021/cs400624c.
[32] W. Yao, Y. Zhang, X. Jia, Z. Huang, Selective catalytic transfer dehydrogenation of alkanes and heterocycles by an iridium pincer complex, Angew. Chem. Int. Ed. 53 (2014) 1390–1394, https://doi.org/10.1002/anie.201306559.
[33] S. Chakraborty, J.A. Krause, H. Guan, Hydrosilylation of aldehydes and ketones catalyzed by nickel PCP-pincer hydride complexes, Organometallics 28 (2009) 582–586, https://doi.org/10.1021/om800948f.
[34] R.B. Leveson-Gower, P.B. Webb, D.B. Cordes, A.M.Z. Slawin, D.M. Smith, R. P. Tooze, J. Liu, Synthesis, characterization, and catalytic properties of iridium pincer complexes containing NH Linkers, Organometallics 37 (2018) 30–39, https://doi.org/10.1021/acs.organomet.7b00713.
[35] L.M. Kumar, B.R. Bhat, Cobalt pincer complex catalyzed suzuki-miyaura cross coupling – a green approach, J. Organomet. Chem. 827 (2017) 41–48, https://doi.org/10.1016/j.jorganchem.2016.11.005.
[36] O.V. Ozerov, C. Guo, B.M. Foxman, Missing link: PCP pincer ligands containing P–N bonds and their Pd complexes, J. Organomet. Chem. 691 (2006) 4802–4806, https://doi.org/10.1016/j.jorganchem.2006.07.018.
[37] I. Göttker-Schnetmann, P. White, M. Brookhart, Iridium Bis(phosphinite) *p*-XPCP pincer complexes: highly active catalysts for the transfer dehydrogenation of alkanes, J. Am. Chem. Soc. 126 (2004) 1804–1811, https://doi.org/10.1021/ja0385235.
[38] D. Benito-Garagorri, V. Bocokić, K. Mereiter, K. Kirchner, A modular approach to achiral and chiral nickel(II), palladium(II), and platinum(II) PCP pincer complexes based on diaminobenzenes, Organometallics 25 (2006) 3817–3823, https://doi.org/10.1021/om060289e.
[39] N.H. Anderson, J. Boncella, A.M. Tondreau, Manganese-mediated formic acid dehydrogenation, Chem. Eur. J. 25 (2019) 10557–10560, https://doi.org/10.1002/chem.201901177.
[40] F. Fang, J.X. Kang, C.Q. Xu, J. Chang, J. Zhang, S. Li, X. Chen, Which type of pincer complex is thermodynamically more stable? Understanding the structures and relative bond strengths of group 10 metal complexes supported by benzene-based PYCYP pincer ligands, Inorg. Chem. 60 (2021) 18924–18937, https://doi.org/10.1021/acs.inorgchem.1c02722.
[41] F. Fang, J. Chang, J. Kang, J. Zhang, S. Li, X. Chen, A structure comparison of Ni(II) complexes supported by PNCNP and POCOP pincer ligands, ChemistrySelect 5 (2020) 5205–5209, https://doi.org/10.1002/slct.202001413.
[42] J. Choi, A.H.R. MacArthur, M. Brookhart, A.S. Goldman, Dehydrogenation and related reactions catalyzed by iridium pincer complexes, Chem. Rev. 111 (2011) 1761–1779, https://doi.org/10.1021/cr1003503.